AEGC2019 Data to Discovery
Australasian Exploration Geoscience Conference
2-5 September 2019 • Perth, Western Australia
Incorporating the AIG, ASEG, PESA, and WABS

Overly steep decays in airborne TEM data and their link to chargeability: example from the Howards East District, NT, Australia

Klara Steklova*
Aarhus University
8000 Aarhus C- DK
klara.steklova@geo.au.dk

Ken Lawrie
Geoscience Australia
GPO Box 378, ACT 2601
ken.lawrie@ga.gov.au

Esben Auken
Aarhus University
8000 Aarhus C- DK
auken@geo.au.dk

Anders V. Christiansen
Aarhus University
8000 Aarhus C- DK
anders.vest@geo.au.dk

Gianluca Fiandaca
Aarhus University
8000 Aarhus C- DK
gianluca.fiandaca@geo.au.dk

SUMMARY

The induced polarization (IP) response in airborne electromagnetic data has recently received attention due to its potential significance for mineral exploration and environmental applications, while also holding the prospect of improved geophysical models. A typical IP response produces negative transients in the late time gates. However, under certain circumstances, the presence of overly steep decays in themselves indicate the presence of chargeable material in the subsurface, i.e. where the chargeability is not strong enough to reverse the sign above the noise level, although it still decreases the signal.

In this contribution, we analyse a survey in the Howards East District in Northern Territory, Australia, and synthetic data. After a standard processing and removal of all noisy and negative data, we proceeded with a standard inversion that resulted in poor fit and unrealistic high resistivity in deeper layers in parts of the survey. Next, we inverted the data with a dispersive earth model, i.e. including the IP parameters. In the parts of the survey where the data could be fitted well with the "resistivity only" inversion the models changed minimally. In the remaining part, mostly with overly steep decays, the inverted models show chargeable, relatively shallow layers, the unrealistic high resistivity was not present anymore and in general, the data residuals dropped to be within the uncertainty of the data.

We further analysed the data, specifically: 1) the soundings linked to chargeable areas; 2) the loss of information due to neglecting the negative or late time data with synthetic models; and 3) we explored the ability of the IP inversion models to recover the moderately chargeable layers. In conclusion, a large-scale airborne IP inversion was executed without any specific processing. Until now a time-consuming specific processing seemed to be a necessary step towards a successful IP inversion with airborne data.

Key words: airborne TEM, induced polarization, field data application, large-scale AEMIP inversion

INTRODUCTION

Recent improvements in Airborne Electromagnetic (AEM) systems, notably in signal to noise ratios, combined with continued improvements in software, indicates that it should be possible to identify/localise chargeable layers in the subsurface, or remove IP effects from the data using airborne IP (AEMIP) inversions. Compared to ground electromagnetic (EM) data, the main challenge in AEM methods is that the amount of data makes any manual processing and inspection impossible or extremely time consuming, hence the determination of IP responses must be automated for any large-scale survey.

Most recent studies of AEMIP have focused on the software and theoretical development of the AIP, such as a reparametrization of the Cole-Cole model to improve the parameter resolution (Fiandaca et al., 2018). Modelling of IP in 1D can be done on a routine basis while in 3D it is more subtle, as the forward modelling is done directly in the time domain. For example, in Marchant et al. (2014) 3D forward modelling is done using a numerical approximation for convolution of Ohm's law.

In Bellivau and Haber (2018), the complex resistivity was replaced by a stretch exponential relaxation, thus making it possible to solve the forward and inverse problems in 3D in the time domain. Another airborne IP inversion approach to estimate a pseudo-chargeability was presented in Kang et al. (2015) and Kang et al. (2017), using data from AeroTEM and VTEM system surveys over a kimberlite complex. In this example, the data responses were decomposed on the fundamental and the IP response, and a 3D pseudo-chargeability was obtained using a linearized inversion approach. The kimberlite complex was also one of the four case studies using 1D based inversion evaluated in Kaminsky and Viezolli (2017). Essentially 1D inversion with spatially constrained regularization reduced the computational burden and improved the resistivity models. In these examples, data processing for the AEMIP inversion was manual, and specific to each field case.

In this present study, the main aim was to test the use of a large-scale airborne IP inversion without the need for any specific processing. More specifically, the aim was to locate any chargeable layers using a more robust approach applicable to large scale surveys. Until now a time-consuming specific processing seemed to be a necessary step towards a successful IP inversion with airborne data.

METHODS

AEM Data Acquisition and Processing

The Howards East District AEM survey was carried out between July 23rd and August 8th 2017, using the SkyTEM 312M *FAST* system. The survey was acquired as part of Geoscience Australia's Exploring for the Future (EFTF) Groundwater Programme. The survey was acquired with a 100 m linespacing over an area of 2074 km near Darwin (Northern Territory, Australia). The main purpose of this survey was to map seawater intrusion along major faults in the Proterozoic Basement. The latter is host to the Howards East aquifer system, which is a major water supply for Darwin and horticulture regionally.

Initially, the AEM field data were inverted with the AarhusInv code (Auken et al., 2015) using the Aarhus Workbench (Auken et al., 2009; www.aarhusgeosoftware.dk). First, raw data stacks from the survey were processed using standard processing of the db/dt data, with coupled, noisy or distorted data culled out. Subsequently, a trapezoidal averaging was applied to the raw data stacks to further reduce the noise, and a standard, resistivity only (RO) inversion was executed. The data uncertainties entering the inversion were estimated from the stacking of the raw transients, with an additional 3% uniform data uncertainty added.

In this study, we used the AEMIP inversion implemented within AarhusInv (Auken et al., 2015) and Aarhus Workbench (Auken et al., 2009). Inverting data does not require a full IP data response with the presence of negative signs in order to invert for IP parameters. We use the maximum phase angle model (MPA), which is a re-parameterization of the Cole-Cole model with parameters – resistivity (ρ), chargeability (*m)*, time constant (τ), and exponent (C) describing the complex resistivity (Fiandaca et al., 2018). To increase the parameters resolution (Lin et al., 2018), the MPA model re-parameterize the Cole-Cole variables as:

$$\tau_\varphi = (1-m)^{1/2C} \ , \ \varphi_{max} = tan^{-1}\left(\frac{\rho''\left(\frac{1}{\tau_\varphi}\right)}{\rho'\left(\frac{1}{\tau_\varphi}\right)}\right)$$

where the ρ', and ρ'' are the real and imaginary part of the complex resistivity. The maximum phase angle, φ_{max}, of the complex conductivity increases with m and C, and thus express the chargeability magnitude in the MPA model, while ρ and C stay defined the same way as in the original Cole-Cole model. For any given set of MPA parameters the corresponding Cole-Cole parameters can easily be obtained and the forward response is calculated with the Cole-Cole model.

The processed data were inverted using the MPA model with the initial model set as a 25 layer, uniform half-space with ρ = 100 Ωm, φ_{max} = 25 mrad, C = 0.3 and τ = 0.001 for all layers. The regularization parameters for the laterally constrained inversion were set as 1.3 and 2 for the lateral and vertical constraints and an a priori constraint of a factor 2 was chosen for φ_{max} and C. The thickness of layers was exponentially growing with depth, with the first layer at 3 metres, and the last, 25th, at 400 m below the surface.

RESULTS

Synthetic Study

To better comprehend the relatively moderate IP response in the Howards East survey, we analysed a "typical" IP response. We chose one of the subareas and selected the models with chargeable layers after the MPA inversion. Generally, 4th to 9th layer (corresponding to roughly 17 down to 50 metres below surface) appears to be the interval with chargeable layers. For the sake of classification we consider as an "IP response" all models that followed these three conditions; 1) the average maximum phase angle, φ_{max}, was higher than 30 mrad, 2) the maximum value in depth profile was higher than 70 mrad and 3) the relative data residual was less than one, that is well fitted data. This filtered out approximately 10 to 20% of soundings as "IP response/ detected", depending on the subarea.

Based on the depth profile of the max phase angle φ_{max} in IP response data, we created a simple three-layer model. We chose the structure of the resistivity model to correspond to the average for the given depth ranges. The three layers thus had resistivities 275, 130 and 460 Ωm with Φ_{max} equal to 36, 55 and 25 mrad in the depth range [17 ,42 and 400] m. As such the second layer is the most conductive and chargeable, while the bottom represents a more resistive layer with (next to no) background chargeability.

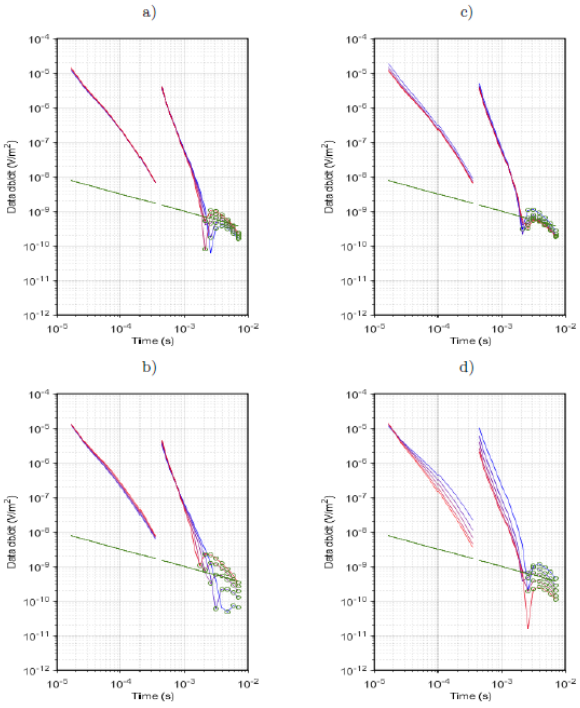

Figure 1. Four different cases of changes from the basic 'typical' IP scenario; a) altering the maximum phase angle of the first and b) second layer, c) altering the resistivity of the first and d) second layer. The negative values are marked with green circles and for clarity are plotted without error bars. A realistic noise level is indicated by the green line.

Afterward, we were altering the resistivity and maximum phase angle values in the first and second layer while keeping the other parameters unchanged. Specifically, ρ_1 as [100,180,27,360,450] Ωm, ρ_2 as [60,95,130,175,210] Ωm,

$\Phi_{max,1}$ as [25,35,45,55,65] mrad and $\Phi_{max,2}$ as [35,45,55,65,75] mrad. The data responses for these essentially 1D layered models are plotted in Figure 1. The simulations show that for most of the data within our survey and within the expected range of parameter values, it is unlikely to get consecutive negative data points in real data impacted by noise.

The 1D scenarios plotted in Figure 1 also provide cases for testing the impact of neglecting the negative data on the inversion estimates by MPA inversion. With random initial half-space models and multiple runs, the mean estimates did not change, and were close to true values in both situations (i.e. all data and positive data only), although as expected, the confidence intervals were wider with reduced (only positive) data. Specifically, the 95% confidence intervals were up to 25% larger for the Φ_{max} estimates and 60 % for the resistivity estimates, though in certain cases have not increased at all. The biggest increase was observed for the highest Φ_{max} in the second layer in scenario in Figure 1b), and for the lowest resistivity values in the second layer in the scenario in Figure 1d). Based on these results, it can be concluded that reducing the IP responses to positive data only does not seem to create a consistently lower or higher estimates.

IP vs RO Inversion

First, we evaluated the standard measures such as mean data residuals, for both the IP and resistivity only (RO) inversion. The obtained range of values confirms the improvement in fit with an IP inversion. The mean residuals for RO inversion were between 1 and 1.2 depending on the subarea, while the IP inversions dropped the mean residual to values between 0.7 and 0.9. However, the improved data fit of IP inversion is more reflected in the percentage of not well fitted data (relative residual higher than 1.1), which is 12% for IP inversion while 30% for RO inversion.

To evaluate how the IP inversion performs in areas, where the RO inversion fits the data well, two groups were identified within the data; the “IP response” (as explained above) and the “mutually good fit” (i.e. where both IP and RO inversions models have a residual less than 1). Afterward, we compared the resistivity models for both IP and RO inversion across the depth profiles. The analysis was carried out separately for all the 6 subareas in our survey to avoid an extensive averaging over possibly different geology. In Figure 2 we show the resulting plot only for one of the subareas. For the data with “mutually good fit” (Figure 2a), the resistivity distribution across the depth for IP and RO inversion are overlapping, though the IP inversion tends to have lower resistivity values. For areas with IP response (Figure 2b), the 50 % confidence intervals are narrower (as it is much smaller area) and overlap in first 20 metres of depth, however, with increasing depth, one can clearly see that the RO inversion produces up to one order higher resistivity values compared to IP inversion. This is expected since the RO inversion attempts to fit the steep decays by very resistive layers in the depth. Last, we compared the maximum phase angle, Φ_{max} for these two data groups. For mutually good fit the Φ_{max} stayed close to the initial value of 25, while for “IP detected” it usually picks maximum values in shallow layers.

To summarize, these plots suggest that the IP inversion does not improve the fit of the data by introducing chargeability where a standard RO inversion fits the data well, and that for these soundings the IP inversion provides similar resistivity models.

Borehole Data

In this study, 27 induction borehole logs were found to have valid data that could be compared with the obtained resistivity models from both IP or resistivity only inversion. Unfortunately, most of the wells do not intersect the IP detected areas and thus cannot provide overall justification for either of the resistivity model estimates. For this study, we selected a profile (part of line 112401), where the IP and RO inversion give significantly different resistivity models and with a borehole location less than 50 m from the line. In the same Figure 3 we also plot the resulting maximum phase Φ_{max} profile. The IP inversion picks a relatively thin but continuous chargeable layer throughout most of the profile. (The connectivity of chargeable layers was also observed in 2D maps for the whole survey). Due to the presence of a chargeable layer, the resistivity model computed by IP inversion has much lower contrast compared to resistivity inversion only, with less conductive sub-surface layers and no extremely resistive layers in large depths. The induction borehole log in the east part does not suggest any extremely resistive material ~60 metres below sub-surface and is therefore more in agreement with IP inversion estimates. This supports the conclusion that we obtain a more realistic geophysical model while also improving the data fit.

CONCLUSIONS

In this study we used a dispersive earth model to invert a large- scale field survey, while applying only a standard processing of the raw data. We demonstrate on synthetic examples that for moderate IP signals, the information about chargeability can be often neglected due to sparse presence of negative data above the noise level.

In the case of Howard river survey, the AEMIP inversion was executed without any specific data processing. The AEMIP inversion improved the data fit so that it is within the data noise levels. The obtained resistivity models are more realistic and in accordance with relevant borehole data. Thus, in certain cases, overly steep decays might be the only indicator of IP phenomena, yet still enable an AEMIP inversion to be performed successfully.

ACKNOWLEDGEMENTS

Niels B. Christensen is thanked for extensive discussions and useful suggestions. This paper is published with permission of the CEO, Geoscience Australia.

REFERENCES

Auken, E., Christiansen, A. V., Kirkegaard, C., Fiandaca, G., Schamper, C., Behroozmand, A. A. and Sørensen, K. (2015). An overview of a highly versatile forward and stable inverse algorithm for airborne, ground-based and borehole electromagnetic and electric data. Exploration Geophysics, 46(3), 223-235.

Belliveau, P., and Haber, E. (2018). Coupled simulation of electromagnetic induction and induced polarization effects using stretched exponential relaxation. Geophysics, 83(2), WB109-WB121.

Fiandaca, G., Madsen, L. M., and Maurya, P. K. (2018). Re-parameterisations of the Cole–Cole model for improved spectral inversion of induced polarization data. Near Surface Geophysics, 16(4), 385-399.

Kaminski, V. and Viezzoli, A. (2017). Modeling induced polarization effects in helicopter time-domain electromagnetic data: Field case studies. Geophysics, 82(2), B49-B61.

Kang, S., Oldenburg, D. W., and McMillan, M. S. (2015). 3D IP inversion of airborne EM data at Tli Kwi Cho. ASEG Extended Abstracts, 2015(1), 1-4.

Kang, S., Fournier, D., and Oldenburg, D. W. (2017). Inversion of airborne geophysics over the DO-27/DO-18 kimberlites—Part 3: Induced polarization. Interpretation, 5(3), T327-T340.

Kratzer, T. and Macnae, J. C. (2012). Induced polarization in airborne EMInduced polarization in airborne EM. Geophysics, 77(5), E317-E327.

Marchant, D., Haber, E., and Oldenburg, D. W. (2014). Three-dimensional modeling of IP effects in time-domain electromagnetic data. Geophysics, 79(6), E303-E314.

Lin, C., Fiandaca, G., Auken, E., Antonio Couto, M., and Christiansen, A. V. (2018). A discussion of 2D induced polarization effects in airborne electromagnetic and inversion with a robust 1D laterally constrained inversion scheme. Geophysics, 84(2), 1-51.

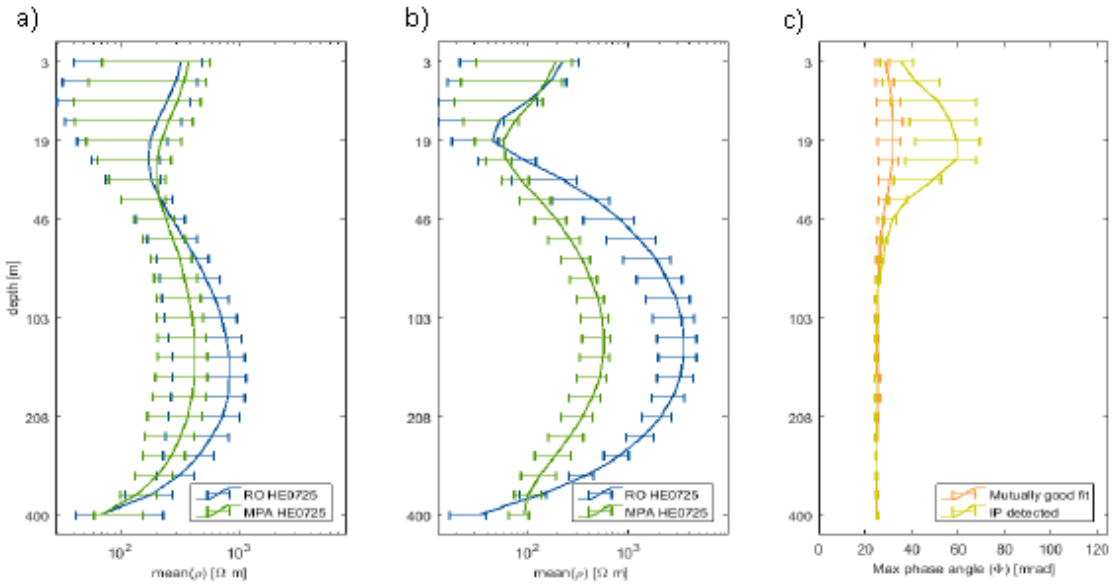

Figure 2. a) The depth profiles for resistivity in areas with good fit for both IP (green) and RO (blue) inversion; b) the resistivity profiles for locations with chargeable anomalies ('IP detected'), c) the depth profiles of maximum phase angle with IP inversion, for mutually good fit (orange) and 'IP detected' zones (yellow). 50% confidence intervals are plotted for all estimates.

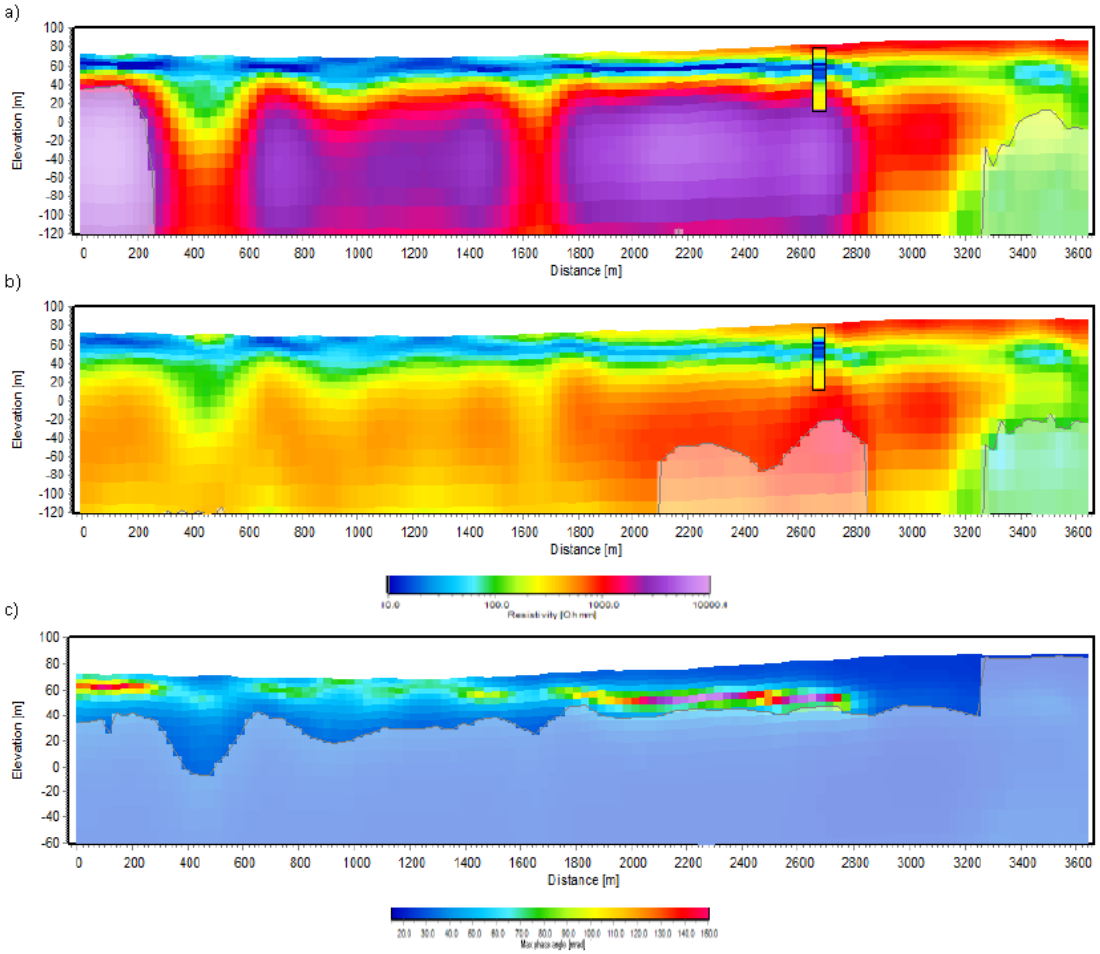

Figure 3. First 3km of the Line 112401. Top panel shows the RO inversion resistivity profile, second panel the MPA resistivity profile, with the well RN 021012. The bottom panel shows the maximum phase angle for the MPA inversion. A borehole with resistivity information is plotted on top.